https://doi.org/10.31436/iiumej.v27i2.3982

Steering Control Precision in Rack Steering Vehicles Using Finite-Time Prescribed Performance Anti-Windup PI Controller with Nonlinear Error Transformation

ADDIE IRAWAN[1*], NORSHARIMIE MAT ADAM[1], R.M.T. RAJA ISMAIL[1], ALIZA CHE AMRAN[2], MOHD ISKANDAR PUTRA AZAHAR[1]

[1]*Robotics, Intelligent Systems and Control Engineering (RiSC) Research Group, Faculty of Electrical & Electronics Engineering Technology, Universiti Malaysia Pahang Al-Sultan Abdullah, Pahang, Malaysia.*
[2]*Motion Control Research Group (MCON), Fakulti Teknologi dan Kejuruteraan Elektrik (FTKE), Universiti Teknikal Malaysia Melaka (UTeM), Melaka, Malaysia.*

**Corresponding author: addieirawan@umpsa.edu.my*

(Received: 13 October 2025; Accepted: 22 January 2026; Published online: 10 May 2026)

ABSTRACT: This paper addresses the challenge of maintaining steering precision and yaw stability in rack steering vehicles (RSVs) operating under varying inertial loads and aerodynamic disturbances. Conventional control methods often struggle to ensure bounded tracking performance in the presence of actuator saturation and nonlinear dynamics. To overcome these limitations, a Finite-Time Prescribed Performance Anti-Windup PI Controller with Nonlinear Error Transformation (FPPC-API-NET) is proposed. The outer loop employs a finite-time prescribed performance framework with a nonlinear transformation to constrain the error trajectory within predefined decay envelopes, while the inner loop incorporates antiwindup compensation to mitigate actuator saturation effects. Simulation studies benchmarked against the FTPPC-API and API controllers demonstrate that FPPC-API-NET achieves up to a 95% reduction in steady-state error, a 70% reduction in settling time, and a 87% reduction in transient duration. The proposed method also enhances yaw stability, reduces lateral displacement by 35%, minimizes sideslip magnitude, and maintains tire-friction utilization below saturation, resulting in smoother lateral acceleration with up to 48% lower peaks. These results confirm that FPPC-API-NET offers superior robustness and precision during cornering maneuvers across varying inertia levels.

ABSTRAK: Kajian ini membincangkan cabaran dalam mengekalkan ketepatan kawalan stereng dan kestabilan sudut gerakan sisi bagi kenderaan jenis rak stering (RSV) yang beroperasi di bawah beban inersia berubah serta gangguan aerodinamik. Kaedah kawalan konvensional sering menghadapi kesukaran mengekalkan prestasi penjejakan apabila berlaku ketepuan aktuator dan kesan dinamik tak linear. Bagi mengatasi kekurangan ini, satu pengawal tirus berasaskan Finite-Time Prescribed Performance dengan Transformasi Ralat Tak Linear dan Antiwindup PI (FPPC-API-NET) telah dicadangkan. Gelung luar menggunakan rangka kerja prestasi terpiawai had masa dengan transformasi ralat tak linear bagi mengehadkan trajektori ralat dalam sempadan peluruhan yang ditetapkan, manakala gelung dalam aplikasi pampasan antiwindup bagi mengawal kesan ketepuan aktuator. Kajian simulasi berbanding pengawal FTPPC-API dan API menunjukkan bahawa FPPC-API-NET mencapai pengurangan ralat keadaan tunak sehingga 95%, masa penetapan 70% lebih pantas, dan tempoh peralihan 87% lebih singkat. Kaedah ini turut meningkatkan kestabilan gerakan sisi, mengurangkan anjakan lateral sebanyak 35%, meminimumkan gelinciran, serta mengekalkan penggunaan geseran tayar di bawah had ketepuan, sekali gus membuktikan

https://doi.org/10.31436/iiumej.v27i2.3982

keteguhan dan ketepatan unggul FPPC-API-NET dalam manuver membelok di bawah variasi inersia.

KEYWORDS: *Rack steering vehicle, prescribed performance control, nonlinear error transformation, inertial variation, cornering path.*

1. INTRODUCTION

Electric vehicles (EVs) and autonomous vehicles (AVs) introduce unique challenges in steering and lateral motion control. The instantaneous torque response and low center of gravity in EV platforms enhance maneuverability but can also exacerbate oversteering and yaw instability during aggressive cornering maneuvers. Meanwhile, AV systems must not only achieve accurate trajectory tracking but also operate reliably in the presence of sensor noise, actuation delays, and environmental uncertainties. These requirements demand steering control architectures that guarantee bounded tracking performance, robustness to inertial variations, and reliable operation under actuator constraints, particularly under high-curvature driving conditions.

To address these challenges, a wide range of vehicle control strategies has been investigated. Among the most established approaches are Model Predictive Control (MPC) [1], sliding mode control (SMC), and Takagi-Sugeno (T-S) fuzzy logic systems [2]. These frameworks have been further enhanced through the integration of intelligent techniques such as neural networks, reinforcement learning, and observer-based designs to accommodate uncertainties and time-varying dynamics [3]. Despite their effectiveness in simulation studies, many of these methods rely on simplified assumptions and often fail to adequately capture practical limitations such as actuator saturation, structural nonlinearities, and sensor bandwidth constraints, which can significantly degrade real-world performance.

Another limitation of many existing steering control approaches is their narrow focus on either stability or tracking performance, frequently overlooking robustness to disturbances, fault resilience, and implementation feasibility. Although integrated control schemes that combine steering, braking, and drive torque have been proposed, their practical deployment is often limited by high computational complexity and system integration challenges. Active Front Steering (AFS), a widely studied technique, improves steering responsiveness but is highly sensitive to inertial effects during sharp cornering, particularly in rack steering vehicle (RSV) systems [4]. Recent advances have introduced coordinated ESP+AFS controllers using variable sliding models to enhance lateral stability under low-adhesion conditions [5]. Comparative studies among AFS, front-wheel independent steering (FWIS), four-wheel steering (4WS), and four-wheel independent steering (4WIS) further indicate that FWIS and 4WIS architectures outperform conventional AFS in yaw rate regulation and path-tracking performance under nonlinear dynamics [6].

Managing inertia-induced instability during cornering remains a persistent and underexplored challenge in RSV dynamics. Rapid steering inputs generate large lateral loads that can lead to vehicle sideslips, loss of tracking accuracy, and, in extreme cases, complete destabilization. Traditional control strategies are often insufficient to mitigate these inertial effects. Rsetam et al. suggested that impedance-based control techniques can improve steering response by modulating control input according to environmental interaction, making them suitable for systems affected by aerodynamic drag and road surface variation [7].

Another promising direction involves the application of Super-Twisting Sliding Mode Control (ST-SMC), which decouples lateral and longitudinal dynamics to enhance robustness

to inertia-driven disturbances [8]. Integrated control strategies combining AFS with direct yaw moment control (DYC) have demonstrated improved lateral stabilization performance [9], while inertial delay control-based sliding mode controllers for 4WS systems with variable steering ratios have been shown to enhance yaw stability under uncertain tire cornering stiffness. In addition, robust output-feedback control designs for AFS have been proposed to mitigate side-wind disturbances and parameter uncertainties, thereby improving lateral stability margins [10].

In parallel, Prescribed Performance Control (PPC) has gained increasing attention as a systematic framework for guaranteeing system performance within predefined error boundaries, even in the presence of disturbances and uncertainties. Finite-time PPC strategies have been successfully applied to steer-by-wire systems [11], while fault-tolerant PPC schemes incorporating fuzzy logic have demonstrated improved reliability under actuator faults [12]. Gao et al. proposed a finite-time PPC strategy for vehicular platoons that ensures bounded tracking and spacing errors [13], whereas Nguyen et al. developed an event-triggered PPC framework with disturbance observers to address electro-hydraulic actuation delays [14].

Further refinements have been achieved by incorporating high-gain observers, adaptive sliding-mode control, and dynamic threshold strategies to enhance tracking performance [13]. Despite these advances, Proportional–Integral–Derivative (PID) controllers remain widely adopted in steering systems due to their simplicity and ease of implementation. However, conventional PID controllers often lack robustness in handling actuator saturation and highly nonlinear vehicle behavior. Anti-windup compensation techniques have been introduced to alleviate integrator saturation, while vector-field methods and intelligent optimization have been employed to enhance PID performance in various steering and motion control applications [15,16].

Therefore, this study addresses the control challenges associated with steering precision and yaw regulation in rack-steering vehicles, particularly under high-curvature cornering conditions, where oversteering and inertia-induced instability are most prevalent. A novel control framework is proposed that integrates Finite-Time Prescribed Performance Control (FTPPC), based on [17], with an Anti-Windup Proportional–Integral (AW-PI) structure and a bounded Nonlinear Error Transformation (NET). Unlike existing hybrid MPC- or SMC-based approaches that often require model inversion, discontinuous control actions, or high computational effort, the proposed FPPC-API-NET achieves finite-time convergence using smooth, bounded transformations while explicitly addressing actuator saturation. Moreover, this proposed control framework is evaluated through comprehensive numerical simulations using a nonlinear RSV dynamic model, thereby enabling a systematic assessment of steering precision and yaw stability under variations in inertia and aerodynamic disturbances. Owing to its algebraic nonlinear transformations and PI-based structure, the proposed controller is computationally lightweight and suitable for real-time embedded automotive implementation, although experimental validation is beyond the scope of this study.

The remainder of this paper is structured as follows. Section 2 presents the dynamic modeling of the RSV, including the Dugoff tire formulation and the coupled yaw–lateral–roll motion equations. Section 3 describes the formulation of the proposed FPPC-API-NET, detailing the control architecture, constraint handling, and nonlinear transformation laws. Section 4 presents simulation results and a comparative performance analysis of FPPC-API-NET, FTPPC-API, and API controllers under varying inertial and aerodynamic conditions. Finally, Section 5 summarizes the key findings and outlines directions for future research.

https://doi.org/10.31436/iiumej.v27i2.3982

2. CONTROLLER DESIGN

This study adopts a cascaded two-loop steering-position controller for RSV's steering-angle control. The outer loop implements an adaptive FT-PPC to target the transformation of the steering angular error, while the inner loop employs an Anti-windup PI (AW-PI) controller to regulate the steering angular position based on the transformed errors. The proposed cascaded controller enforces error constraints using a tunable prescribed performance function, while the anti-windup function ensures robustness against saturation.

2.1. Overview of Steering Vehicle Dynamics

The RSV is modeled to capture the essential dynamics governing interactions among steering, yaw, and roll. The model employs the Dugoff tire formulation to describe nonlinear longitudinal and lateral tire forces, while the vehicle states are defined by the sideslip angle, β, yaw rate, $\dot{\psi}$, and roll angle, ϕ . The overall system coordination, including the vehicle motion, reference axes, and tire dynamics, is depicted in Fig. 1.

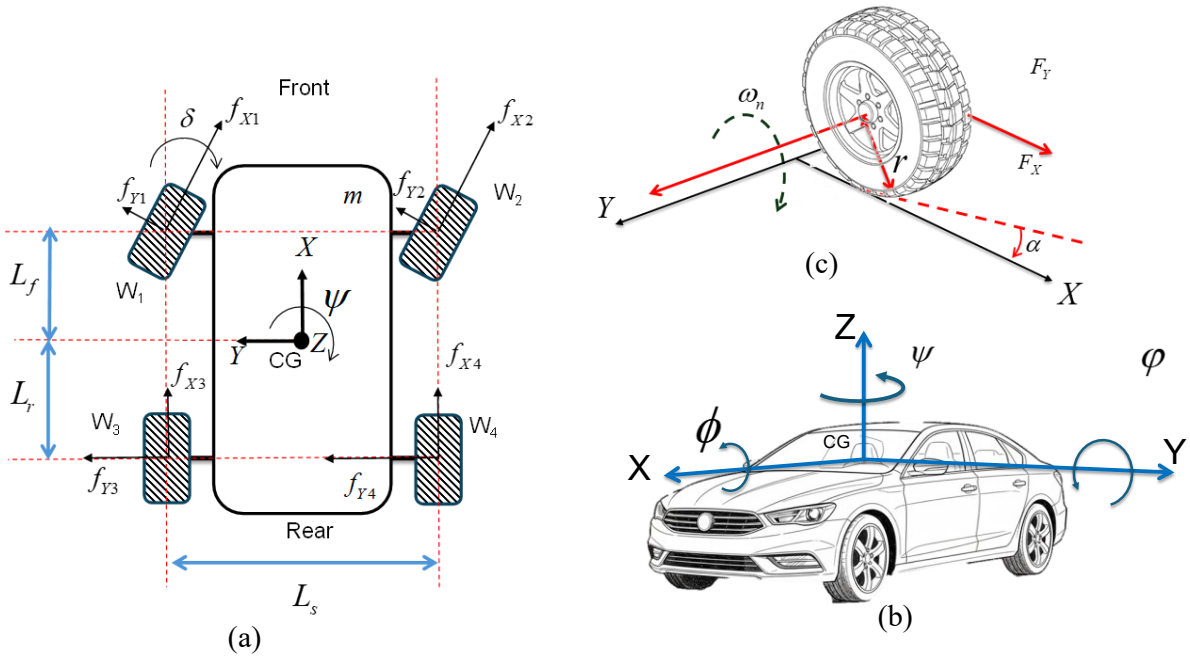

Figure 1. RSV system coordination, (a) vehicle dynamics motion, (b) vehicle axis system, and (c) tire dynamics motion.

The kinematic accelerations in the inertial frame are expressed as follows:

$$a_x = \dot{V}_x - \dot{\psi}V_y, \quad a_y = \dot{V}_y - \dot{\psi}V_x \tag{1}$$

Then, the slip angles of the front and rear tires, which directly influence the lateral forces, are given by

$$a_f = \delta_f - \arctan\left(\frac{V_y + L_f\dot{\psi}}{V_x}\right), \quad a_r = -\arctan\left(\frac{V_y - L_r\dot{\psi}}{V_x}\right) \tag{2}$$

where δ_r is the steering input, L_f and L_r are the distances from the vehicle center of gravity (CG) to the front and rear axles, respectively. The Dugoff tire model [18] provides the longitudinal and lateral forces as:

$$F_x = C_\sigma \sigma_x f(\lambda), \quad F_y = C_\alpha \tan\alpha f(\lambda) \tag{3}$$

https://doi.org/10.31436/iiumej.v27i2.3982

where C_σ and C_α are longitudinal and cornering stiffness coefficients, respectively, σ_x is the longitudinal slip ratio, and $f(\lambda)$ is a nonlinear saturation function dependent on the road–tire friction coefficient, μ. The parameters used in this RSV dynamic model are summarized in Table 1 and are adopted from established Dugoff tire–based vehicle models in the [18,19]. The listed parameters represent the physical properties, stiffness coefficients, geometric dimensions, and inertial constants governing the vehicle's behavior under steering motion.

The longitudinal slip ratio is defined as follows:

$$\sigma_x = \begin{cases} \frac{r\omega - V_x}{r\omega}, & acceleration \\ \frac{V_x - r\omega}{V_x}, & braking \end{cases} \tag{4}$$

with r denoting the tire radius and ω is the wheel's angular velocity and $n = 1,2,\ldots,4$ is the number of wheels as depicted in Fig.1(c). The yaw moment balance around the vertical axis is expressed as follows:

$$I_x\ddot{\psi} + I_{xz}\ddot{\phi}_v = \sum M_{z,i} \tag{5}$$

where I_z is the yaw inertia and I_{xz} is the cross-inertia coupling between yaw and roll. The roll dynamics are described by

$$I_{xx}\ddot{\phi} + C_\phi\dot{\phi}_v + K_\phi\phi_v = m_s h a_y \tag{6}$$

where I_{xx} is roll inertia, C_ϕ and K_ϕ are the suspension damping and stiffness coefficients, m_s is the spring-mass, and h, is the height of the center of gravity.

Table 1. List of RSV's parameters and coefficients

Definition	Symbol	Value
Vehicle mass	m	1300 kg
Longitudinal stiffness	C_σ	20000 N/rad
Cornering stiffness	C_α	80000 N/rad
Distance of front axle from CoG	L_f	1.180 m
Distance of rear axle from CoG	L_r	1.770 m
Track width between left and right wheels	L_s	1.880 m
Acceleration due to gravity	g	9.81 m/s²
Tire radius (effective)	r	0.38m
Tire–road friction coefficient	μ	0.85
Yaw moment of inertia	I_z	2480 kg·m²

By applying small-angle approximations to the slip angles and assuming constant longitudinal velocity, the system reduces to the well-known bicycle model, expressed as

$$\dot{\beta} = -\left(\frac{C_f + C_r}{mV_x}\right)\beta + \left(\frac{C_r L_r - C_f L_f}{mV_x^2} - 1\right)\dot{\psi} + \left(\frac{C_f}{mV_x}\right)\delta_f \tag{7}$$

$$\ddot{\psi} = \left(\frac{C_f L_f - C_r L_r}{I_x}\right)\beta - \left(\frac{C_f L_f^2 - C_2 L_r^2}{I_z V_z}\right)\dot{\psi} + \left(\frac{L_f C_f}{I_z}\right)\delta_f \tag{8}$$

where C_f and $C_r$denote the front and rear cornering stiffness, respectively, and m, is the vehicle mass. The complete RSV dynamic model structure, incorporating the Dugoff tire formulation and the lateral–yaw–roll interaction, is illustrated in Fig. 2. This figure highlights the integration of subsystems such as tire dynamics, yaw and roll coupling, and the vehicle motion response, which collectively represent the plant used in the proposed control design.

https://doi.org/10.31436/iiumej.v27i2.3982

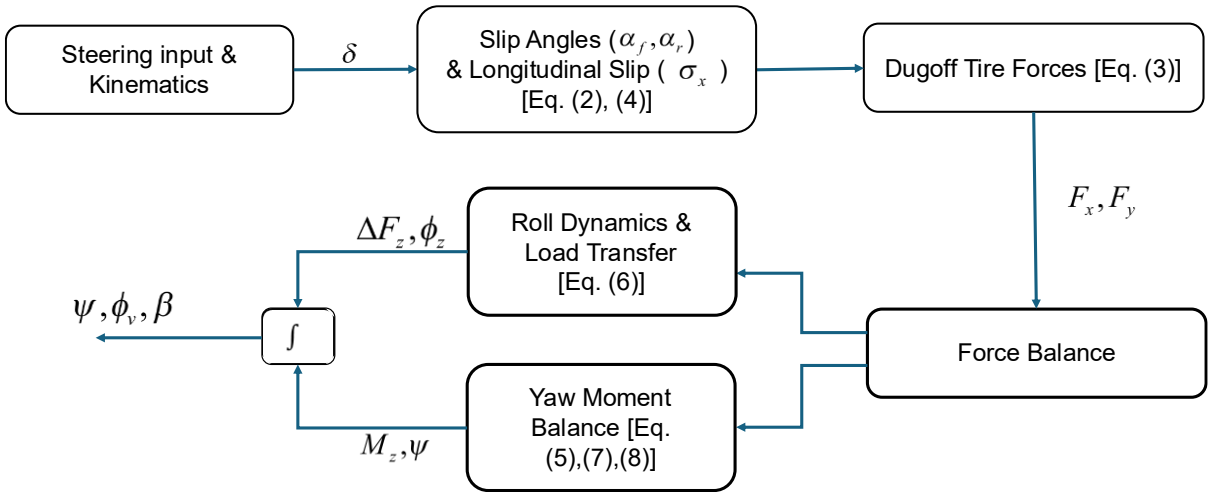

Figure 2. Overall structure of the RSV dynamics model

2.2. Problem Formulations

Let the yaw angle output be ψ and reference be ψ_r. Define yaw tracking error as follows:

$$e_\psi(t) = \psi_r(t) - \psi(t) \tag{9}$$

Adopt the prescribed performance function (PPF) [17] as follows:

$$\rho(t) = (\rho_0 - \rho_\infty)e^{-\frac{t^2}{2\left(\frac{t_c}{2}\right)^2}} + \rho_\infty, \ \ \rho_0 > \rho_\infty > 0, t_c > 0, \tag{10}$$

and form the normalized and transformed errors as follows:

$$\Delta(t) = \frac{e_\psi}{\rho(t)}, \quad \varepsilon(t) = \frac{1}{2}\ln\left(\frac{1+\Delta(t)}{1-\Delta(t)}\right) \tag{11}$$

Then, differentiation gives

$$\dot{\varepsilon}(t) = \frac{1}{1-\Delta^2(t)}\left(\frac{\dot{e}_\psi(t)}{\rho(t)} - \Delta(t)\frac{\dot{\rho}(t)}{\rho(t)}\right) \tag{12}$$

where $\dot{e}_\psi$ is the yaw error rate that can be expressed as follows:

$$\dot{e}_\psi(t) = \dot{\psi}_r(t) - \dot{\psi}(t) \tag{13}$$

with $\dot{\psi}_r$ is the reference for the vehicle's yaw rate.

2.3. Finite-Time Prescribed Performance Anti-Windup PI Controller with Nonlinear Error Transformation

Starting from the prescribed performance function, $\rho(t)$ and the transformed error, $\varepsilon(t)$, defined in Eqs. (10)-(12), the control objective is to ensure that the yaw tracking error remains strictly within the prescribed performance bounds while generating a steering command that respects actuator limitations. In practical rack steering systems, direct inversion of the steering–yaw dynamics, or aggressive high-gain control, may lead to actuator saturation, excessive control effort, or degraded robustness. Therefore, instead of explicitly inverting the system dynamics, the proposed approach shapes the steering correction as a smooth nonlinear function of the transformed error, enabling finite-time convergence while preserving bounded control authority.

https://doi.org/10.31436/iiumej.v27i2.3982

Conventional prescribed performance control schemes commonly employ logarithmic or unbounded power-based error transformations to enforce performance constraints [17]. Although effective in theory, such transformations may produce excessively large control signals when the transformed error grows, particularly during large transients or under inertia variation. This behavior is undesirable in rack-steering vehicles, where physical steering limits and actuator saturation must be explicitly accounted for. To address this limitation, a bounded Nonlinear Error Transformation (NET) is introduced in this study that preserves the sign information of the transformed error while ensuring smooth, bounded control actions.

Specifically, a sign-preserving power of the transformed error is defined as

$$\varepsilon^{\gamma}(t) = sign\big(\varepsilon(t)\big)|\varepsilon(t)|^{\gamma}, \;\; 0 < \gamma \leq 1 \tag{14}$$

which retains sensitivity to small errors while moderating the growth rate for large error magnitudes. This transformed error is then mapped to the steering domain through a bounded and monotonic nonlinear function given by

$$\delta_{fb}(t) = \Delta_{max} \tanh\left(\frac{K_{NET}\varepsilon^{\gamma}(t)}{\Delta_{max}}\right), \qquad K_{NET} > 0, \Delta_{max} > 0 \tag{15}$$

where $\delta_{fb}(t)$ denotes the feedback steering correction, K_{NET} is a positive gain that scales the response near the origin, and Δ_{max} defines the maximum allowable steering correction. The hyperbolic tangent function ensures that the feedback term is odd, strictly increasing, and bounded such that $|\delta_{fb}| \leq \Delta_{max}$, thereby preventing excessive steering commands and preserving actuator safety. For small values of $|\varepsilon(t)|$, the nonlinear function in Eq. (15) can be locally approximated using the first-order Taylor expansion of the hyperbolic tangent function, yielding

$$\delta_{fb}(t) \approx \Delta_{max} K_{NET}\varepsilon^{\gamma}(t) \tag{16}$$

which indicates that K_{NET} governs the proportional response in the vicinity of the equilibrium point. The exponent $\gamma \in (0,1)$ further adjusts the nonlinearity of the transformation, where smaller values of γ enhance sensitivity for small errors and accelerate convergence toward the prescribed performance funnel, while $\gamma = 1$ recovers a linear behavior.

For large values of $|\varepsilon(t)|$, the hyperbolic tangent function smoothly saturates, causing $\delta_{fb}(t)$ to asymptotically approach $\pm\Delta_{max}$. This bounded behavior fundamentally distinguishes the proposed NET from conventional logarithmic or unbounded power-based transformations, as it prevents aggressive transients from demanding excessive steering authority and improves robustness under actuator saturation.

To ensure a finite slope at the origin when $\gamma < 1$, a regularized form of the power function may be employed

$$\varepsilon_{\gamma,\delta}(t) = sign\big(\varepsilon(t)\big)[|\varepsilon(t)| + \delta]^{\gamma} \tag{17}$$

which preserves the oddness and boundedness of the transformation while avoiding singular behavior. In this case, $\varepsilon^{\gamma}(t)$ in Eq. (16) is replaced by $\varepsilon_{\gamma,\delta}(t)$. The steering reference is then constructed as the sum of a feedforward term and the bounded feedback component,

$$\delta_v(t) = \delta_r(t) + \delta_{fb}(t) \tag{18}$$

where $\delta_v(t)$ represents a new or dynamically updated desired steering trajectory. Thus, the steering tracking can be expressed as follows, with $\delta(t)$ as a measured feedback steering from the RSV dynamic model [20]:

https://doi.org/10.31436/iiumej.v27i2.3982

$$e_\delta(t) = \delta_v(t) - \delta(t). \tag{19}$$

The inner-loop steering controller employs an anti-windup PI (AW-PI) structure with back-calculation, expressed as

$$\begin{aligned} u_c(t) &= K_p e_\delta(t) + K_i z(t) \\ \dot{z}(t) &= e_\delta(t) + K_b(u(t) - u_c(t)) \\ u(t) &= \Lambda(u_c(t)) \end{aligned} \tag{20}$$

Here, $z(t)$ is the integral state, $K_b > 0$ is the back calculation gain, and $\Lambda(\cdot)$ denotes the actuator map, which may impose magnitude or rate constraints. In the linear operating region, $\Lambda(u_c) = u_c$ and the integrator evolves with $\dot{z} = e_\delta$. When the actuator saturates, the term, $K_b(u - u_c)$, drives the integral state toward the actual actuator signal, which prevents windup and ensures smooth recovery as the actuator reenters its linear range [20]. Finally, $[K_p, K_i] > 0$ are the positive finite design parameters. With the inner loop tuned to track, δ_v, faster than the outer loop, the NET in Eqs. (14)-(18) produces a steering correction that is sign consistent with ε, increases with $|\varepsilon|$, yet remains bounded by Δ_{max}, therefore, the prescribed bound, $|e_\psi| < \rho(t)$ is preserved while respecting steering limits. Fig. 3 shows the overall proposed control system structure with the RSV dynamic model as a plant.

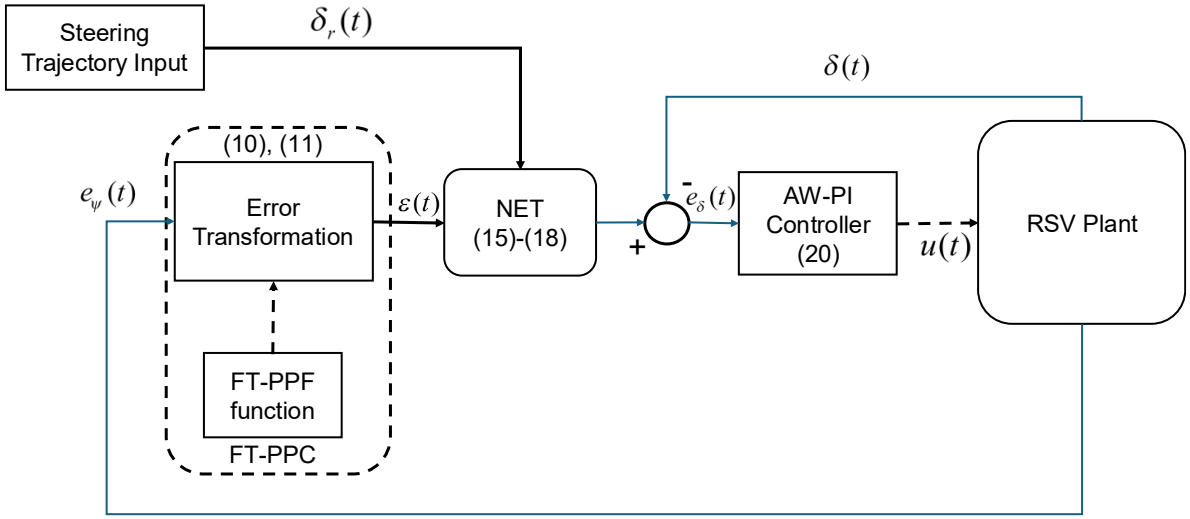

Figure 2. Functional block of FPPC-API-NET for RSV's steering positioning

2.4. Stability Analysis

Consider the $\varepsilon(t)$defined in Eq. (11), which relates to the yaw tracking error, $e_\psi(t)$under the prescribed performance transformation. To verify the stability of the cascaded control framework, define the Lyapunov candidate as

$$V_\varepsilon = \frac{1}{2}\varepsilon^2(t), \tag{21}$$

which is positive definite for all $\varepsilon(t) \neq 0$. Its time derivative along the trajectories of the closed-loop error system is obtained as

$$\dot{V}_\varepsilon = \varepsilon(t)\dot{\varepsilon}(t). \tag{22}$$

From Eq.(12), the derivative of $\varepsilon(t)$can be expressed as

$$\dot{\varepsilon}(t) = \frac{2\dot{e}_\psi(t)}{\rho(t)\left[1-\left(e_\psi(t)/\rho(t)\right)^2\right]} - \frac{2e_\psi(t)\dot{\rho}(t)}{\rho^2(t)\left[1-\left(e_\psi(t)/\rho(t)\right)^2\right]}. \tag{23}$$

Under the outer-loop FT-PPC NET control law Eqs. (15)–(18), the transformed error dynamics can be shaped as

$$\dot{\varepsilon}(t) = -k_\varepsilon(t)\varepsilon(t) + \Delta(t), \tag{24}$$

with $k_\varepsilon > 0$ denotes the adaptive convergence rate determined by the prescribed performance shaping, and $\Delta(t)$ represents bounded residual effects arising from model uncertainties or coupling terms in the RSV dynamics. Substituting this into the Lyapunov derivative yields

$$\dot{V}_\varepsilon(t) = -k_\varepsilon(t)\varepsilon^2(t) + \varepsilon(t)\Delta(t). \tag{25}$$

Since $\Delta(t)$ is bounded, there exists a positive constant, $\gamma > 0$ such that

$$\dot{V}_\varepsilon(t) \leq -\gamma V_\varepsilon(t), \tag{26}$$

which guarantees exponential convergence of $\varepsilon(t)$ to zero. Consequently, the original $e_\delta(t)$, is confined within the prescribed performance envelope, $\rho(t)$ defined in Eq. (10), ensuring finite-time boundedness and overshoot-free tracking. For the inner loop, the AW-PI control law Eq. (20) regulates the steering error, $e_\delta(t)$ with control input, $u_c(t)$ and integrator dynamics, $\dot{z}(t)$. The Lyapunov function is selected as

$$V_\delta(t) = \frac{1}{2}e_\delta^2(t) + \frac{1}{2K_i}z^2(t), \tag{27}$$

whose time derivative along Eq. (20) satisfies

$$V_\delta(t) \leq -K_p e_\delta^2(t) - K_b[u_c(t) - \Lambda(u_c(t))]^2 \leq 0. \tag{28}$$

Hence, $e_\delta(t)$ and $z(t)$ are bounded and converge asymptotically to zero when the actuator operates within its linear range, while the anti-windup term ensures smooth recovery under saturation. Since both subsystems are input-to-state stable (ISS) and the inner loop is designed to respond faster, $T_\delta \ll T_\varepsilon$, the small-gain theorem ensures the stability of the full cascaded system. Therefore, all closed-loop signals are bounded, and the tracking objectives are achieved.

The proposed FPPC-API-NET controller ensures that the transformed error, $\varepsilon(t)$, converges exponentially to zero, maintaining $e_\psi(t)$ strictly within the prescribed bounds. The inner loop guarantees bounded steering control with effective anti-windup compensation. The overall system achieves robust stability and tracking performance in the presence of model uncertainties, actuator saturation, and external disturbances.

3. Results and Discussion

Simulation studies were conducted to assess and verify the proposed FPPC-API-NET controller's ability to regulate steering precision and yaw stability under nonlinear coupling effects. Prior to simulation, the FPPC-API-NET parameters were fine-tuned to satisfy the nonlinear and coupling constraints embedded in its control structure, with both the outer and inner control loops optimized to maintain consistency with the RSV model's nonlinear dynamics. Specifically, the outer-loop finite-time prescribed performance NET was calibrated to ensure strict error confinement within the decaying envelope defined by the nonlinear transformation function, $\rho(t)$, while maintaining smooth convergence under varying inertial and aerodynamic disturbances. Concurrently, the inner anti-windup PI (AW-PI) parameters were tuned via constraint-aware iterations to satisfy actuator saturation limits and the coupling between the steering torque dynamics and the yaw-moment balance described in Eqs. (5)-(8). This parameter adjustment ensured that the nonlinear saturation characteristics in the NET law (Eqs. 15–16) and the feedback regularization in the AW-PI loop (Eq. 20) operated in a

https://doi.org/10.31436/iiumej.v27i2.3982

dynamically coordinated manner, preserving stability and maintaining bounded steering authority within the prescribed performance envelope. The finalized parameter set, summarized in Table 2, represents the optimum balance between transient responsiveness and saturation avoidance, determined through iterative closed-loop validation using the RSV plant. To emulate real on-road conditions, aerodynamic disturbances were introduced into the RSV model within the 9–10 Hz frequency band, along with an additional 100 kg payload to represent inertia-variation effects. The comparative analysis was carried out by benchmarking the proposed controller against the Finite-Time Prescribed Performance with Antiwindup PI (FTPPC-API) and the baseline Antiwindup PI (API) controllers used in previous studies[20].

The steering position tracking responses in Fig. 4 indicate that the proposed FPPC-API-NET achieves the highest closed-loop tracking accuracy and the fastest convergence under varying inertia conditions. The response closely follows the steering reference, exhibits negligible steady-state error, and shows rapid transient decay, with settling occurring at approximately 2 seconds despite the imposed disturbances. The FTPPC-API yields moderate performance with a larger residual steady-state deviation and a longer settling time, while the baseline API exhibits pronounced lag and oscillatory behavior. Quantitatively, FPPC-API-NET reduces the final steady-state error by approximately 68% relative to FPPC-API and nearly 95% relative to API, confirming superior steering-angle regulation and transient suppression.

This improvement is primarily attributed to the decay-function envelope of the prescribed performance function (PPF), as shown in Fig. 3, which dynamically constrains the evolution of the tracking error within predefined boundaries. The smooth funnel-shaped envelope defined by $\rho(t)$ effectively shapes the transient response and limits overshoot while enforcing finite-time convergence.

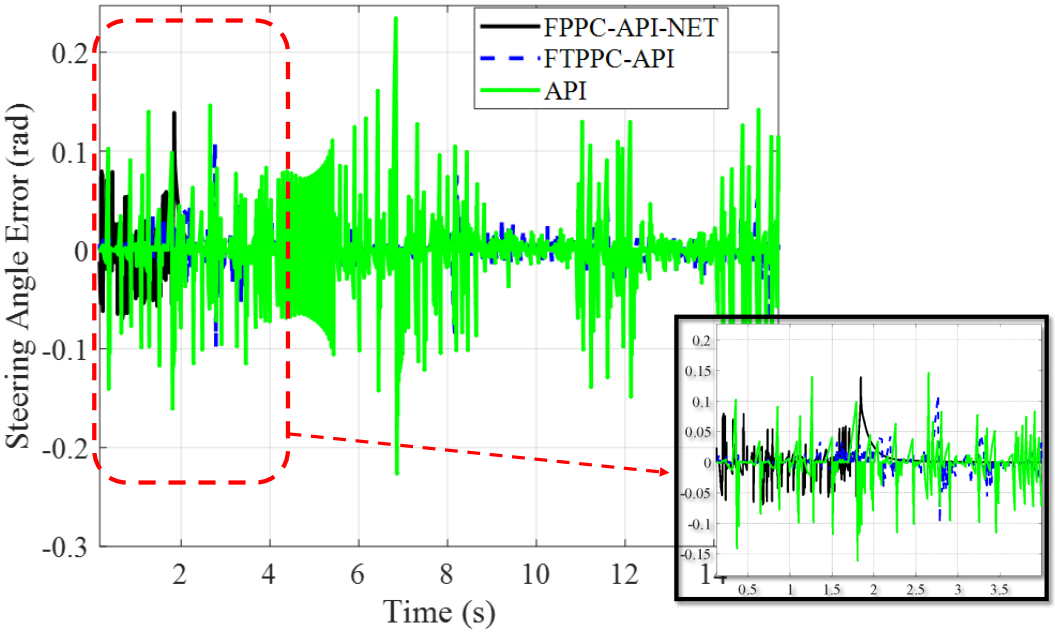

Figure 3. Steering position tracking performances between controllers.

In the FPPC-API-NET, the nonlinear error transformation (NET) acts as an adaptive gain-scaling mechanism that regulates the control effort based on the magnitude of the transformed error, ensuring that large initial deviations produce proportionally stronger corrective actions while small residual errors are attenuated smoothly near convergence. Consequently, the tracking-error trajectory remains strictly confined within the prescribed decay limits throughout the maneuver.

https://doi.org/10.31436/iiumej.v27i2.3982

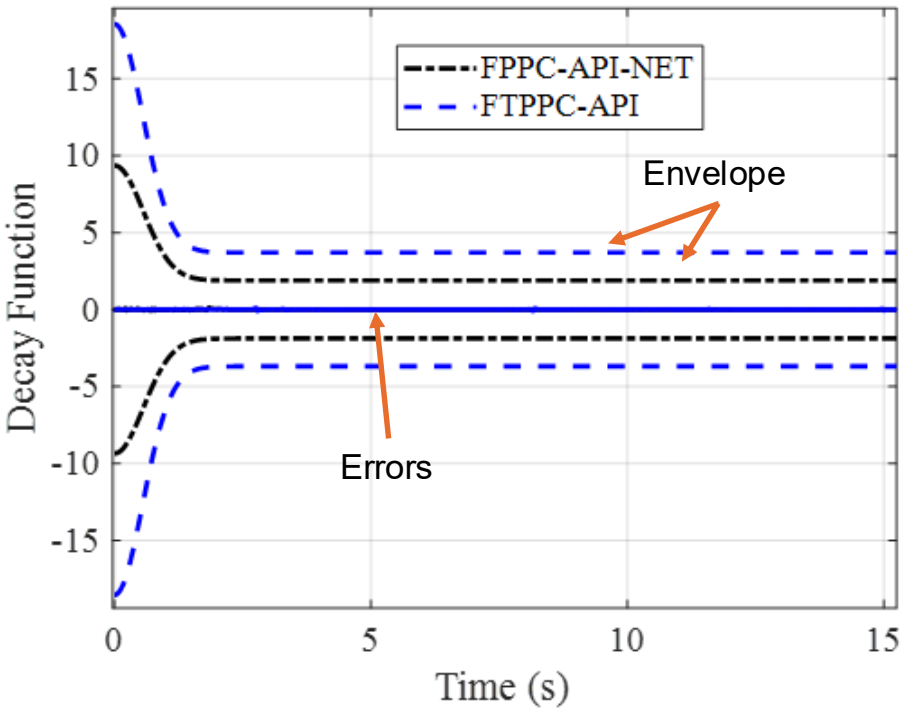

Figure 4. Sample of tracking error in the decay smooth function boundary between FPPC-API-NET and FTPPC-API.

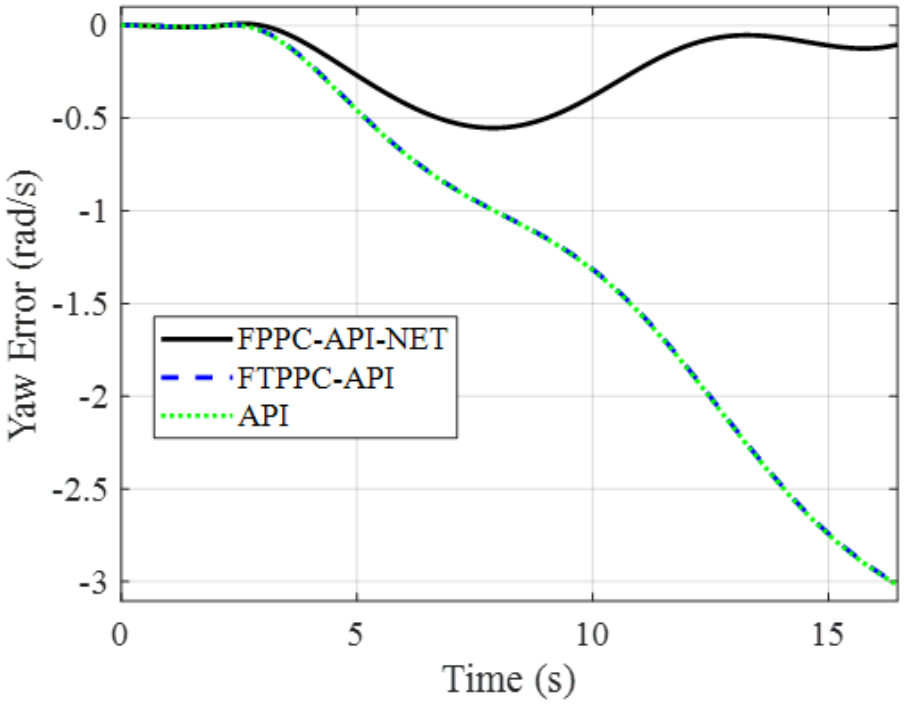

Figure 5. Comparison between controllers in the vehicle's yaw stability margin

Both FPPC-API-NET and FTPPC-API maintain their error trajectories within the respective PPF envelopes. However, the proposed FPPC-API-NET exhibits a narrower performance funnel, approximately 23 % tighter, which imposes stricter error regulation and enhances the convergence rate. The nonlinear transformation further introduces a nonlinear damping effect that improves transient-response uniformity, preventing high-frequency oscillations and reducing the control energy required for error correction. This explains the

https://doi.org/10.31436/iiumej.v27i2.3982

faster convergence and smaller steady-state deviation observed in Fig. 4. Overall, the enhanced steering precision achieved by FPPC-API-NET stems directly from the combined effect of finite-time PPF shaping and bounded NET, which collectively improve control adaptability under varying inertial conditions.

These enhanced steering characteristics directly influence the vehicle's yaw motion, as shown in Fig. 6. FPPC-API-NET maintains stable yaw-rate responses with uniform gain and phase margins across inertia variations, indicating robustness to dynamic parameter changes. The FTPPC-API response, by contrast, exhibits a slower transient response as inertia increases, while the API controller suffers from pronounced overshoot and phase lag, indicating inferior damping and poor stability. FPPC-API-NET's improved damping characteristics mitigate oscillations and preserve bandwidth, confirming that the proposed NET effectively compensates for inertia-induced dynamics, thereby sustaining yaw stability throughout cornering maneuvers.

The effect of improved yaw regulation is further reflected in lateral-displacement performance, presented in Fig. 6. FPPC-API-NET achieves the smallest deviation from the reference path, reducing peak lateral displacement by approximately 35 % compared with FTPPC-API and more than 60 % relative to API. Moreover, FPPC-API-NET exhibits a faster lateral-error decay rate (≈ 40 % improvement), ensuring rapid trajectory recovery following a disturbance. These results highlight the controller's superior capability to manage lateral–yaw coupling through adaptive force redistribution between the front and rear axles.

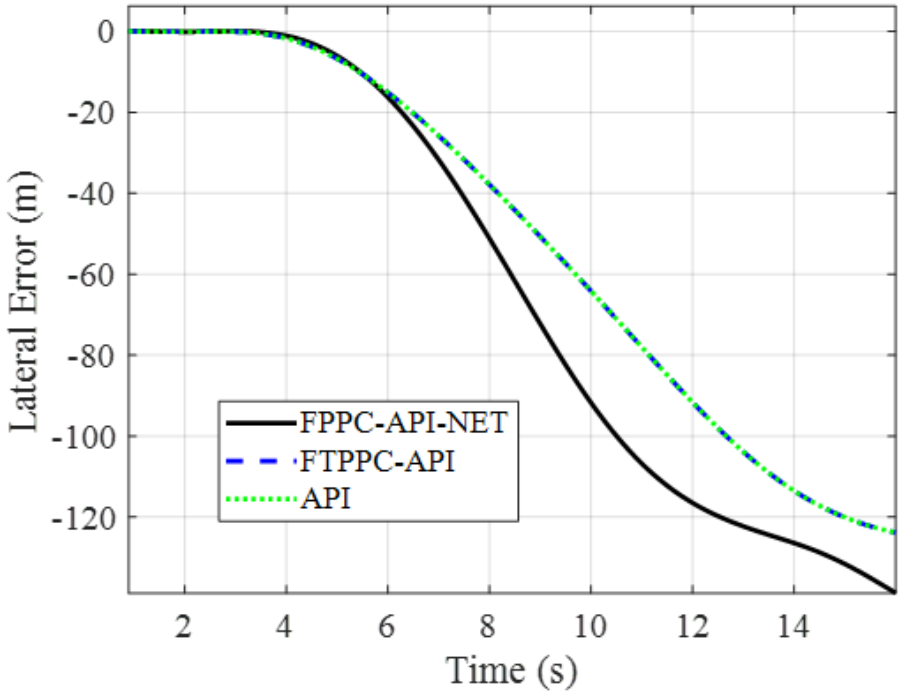

Figure 6. Comparison of the vehicle's lateral displacement errors between controllers.

The tighter integration of the outer PPF layer and the inner anti-windup compensation ensures that transient steering corrections remain dynamically consistent with tire-force limits, maintaining both path-tracking accuracy and yaw stability even under inertia-driven nonlinearities.

Table 2. Fine-tuned Design Parameters

Parameter	FPPC-API-NET	FTPPC-API	API
K_p	15.5017	11.3057	14.0137
K_i	8.7521	1.3935	4.2017
K_b	3.5911	7.5534	0.1
ρ_0	9.3491	16.7776	-
t_c	2.2289	1.2006	-
ρ_∞	1.8855	4.6328	-
K_{NET}	0.0689	-	-
Δ_{max}	0.0478	-	-
γ	0.5360	-	-

Complementary insights are provided by the sideslip dynamics in Figs. 7(a) and 7(b). FPPC-API-NET maintains the lowest sideslip angle, β, magnitude, and a faster sideslip rate, $d\beta/dt$, decay. The settling time of $d\beta/dt$ is approximately 45% shorter than that of FTPPC-API and 70% shorter than API, illustrating enhanced lateral stability and superior disturbance rejection capability. Lower βamplitudes also correspond to improved tire force alignment and reduced lateral drift, confirming the controller's effectiveness in maintaining balanced cornering behavior.

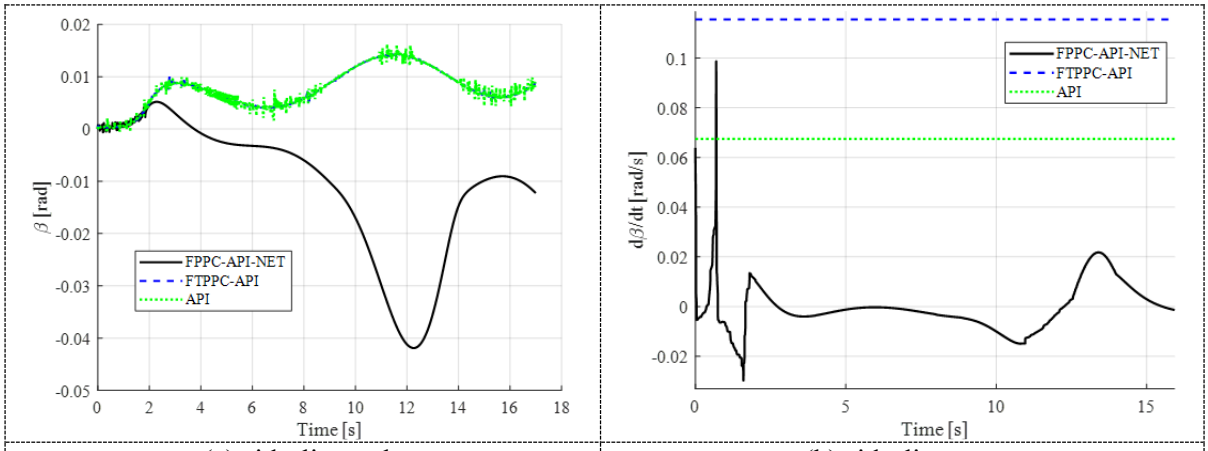

(a) sideslip angle (b) sidesling rate

Figure 7. Comparison between controllers

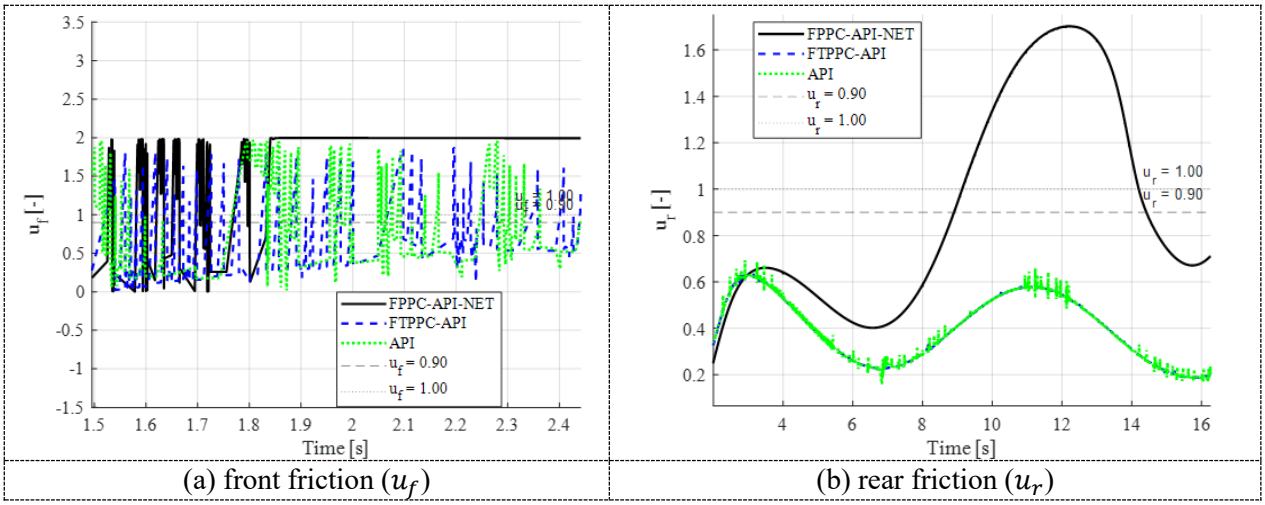

(a) front friction (u_f) (b) rear friction (u_r)

Figure 8. Comparison between the vehicle's front and rear friction utilization.

Further evidence of robustness is provided by the tire-friction utilization results in Figs. 8(a) and 8(b). Both front and rear tires operate within the safe adhesion limit of $\mu = 0.85$, demonstrating that FPPC-API-NET prevents tire saturation during high-curvature maneuvers. The front-tire utilization peak is approximately 0.91 for FPPC-API-NET, compared with 0.96 for FTPPC-API and 1.04 for API. The rear-tire utilization remains near 0.88, indicating balanced load transfer between axles. These findings confirm that the nonlinear error-transformation control law not only enhances steering precision but also maintains efficient friction distribution, resulting in improved cornering stability, lower energy loss, and extended tire lifespan. Although explicit electrical energy consumption is not directly evaluated in this study, the observed reduction in steering command oscillations, lower tire–road friction utilization, and smoother lateral acceleration profiles collectively serve as indirect indicators of improved control efficiency. By preventing excessive corrective steering actions and avoiding tire force saturation during aggressive cornering maneuvers, the proposed FPPC-API-NET reduces unnecessary energy dissipation while maintaining robust lateral stability. These characteristics suggest that the proposed control strategy is well-suited to energy-conscious steering applications, particularly on electric and autonomous vehicle platforms, where efficiency and stability must be considered jointly.

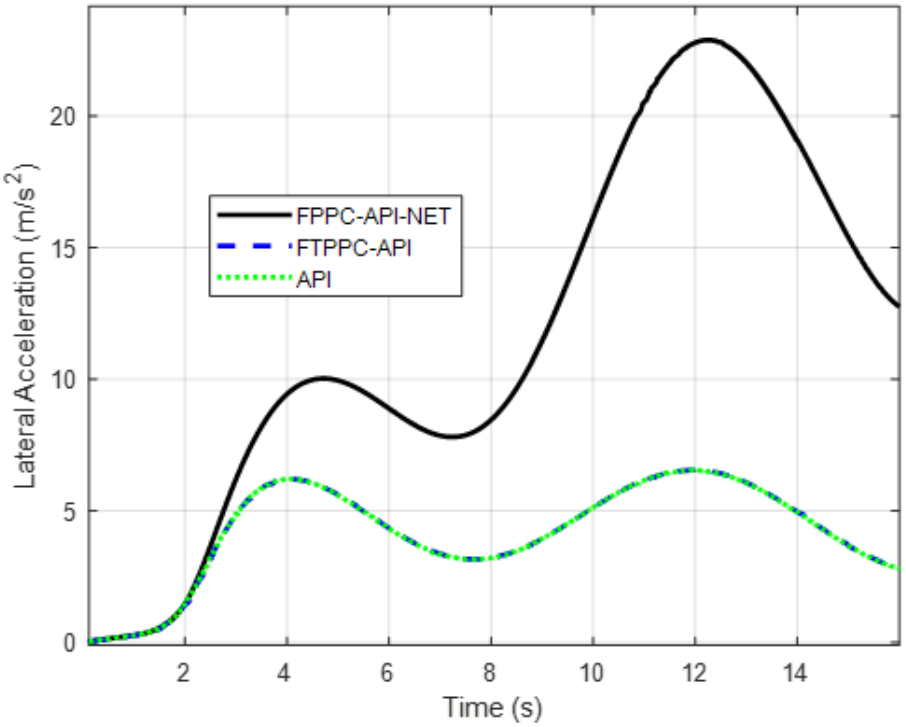

Figure 9. Comparative lateral acceleration responses (a_y), among controllers

This efficiency is also evident in the lateral acceleration, a_y, responses plotted in Fig. 9. FPPC-API-NET delivers smoother acceleration profiles with reduced oscillations and peak magnitudes, achieving approximately 28% lower peak magnitudes than FTPPC-API and 48% lower than API. The smoother $a_y$curves indicate improved ride comfort, reduced dynamic load transfer, and minimized roll excitation, all of which contribute to enhanced handling performance and passenger comfort under varying inertial conditions.

The observed dynamic responses are consistent with the robustness indices summarized in Table 3, which compare transient specifications across controllers. FPPC-API-NET demonstrates a 66.7% faster rise time, a 87.4% shorter transient duration, and a 70% faster

settling time than FPPC-API, while maintaining stable bounded overshoot. Although the overshoot amplitude is approximately 221.8% larger than that of FTPPC-API, it is well-regulated and quickly attenuated within the prescribed performance boundary, reflecting the controller's aggressive yet stable finite-time convergence. The combined results affirm that FPPC-API-NET offers the best trade-off between fast convergence and robust stability across steering and yaw dynamics.

Table 3. Performance and robustness of the controllers

Controller / Parameter	FPPC-API-NET	FTPPC-API	API
Rise Time	0.1 ms	0.3 ms	0.5 ms
Transient Time	2.14 ms	8.18 ms	10.1 ms
Settling Time	2.90 ms	8.18 ms	9.8 ms
Max. Overshoot	6.58 milliradians	1.09 milliradians	460.82 milliradians

Table 4. Overall measurement matrix of controller performance

Metric	FPPC-API-NET	FTPPC-API	API	Improvement (FPPC-API-NET)
Steering steady-state error	Lowest (≈95% ↓ vs API)	Moderate	Highest	95% lower
Tracking error bound	Tightest (23% ↓)	Moderate	Not bounded	23% smaller
Yaw stability margin	High, uniform	Medium, varying	Low	Consistent stability
Lateral displacement peak error	−35%	Moderate	Highest	35% lower
Sideslip angle amplitude	Lowest	Medium	Highest	45–70% faster decay
Tire friction (front/rear)	0.91 / 0.88	0.96 / 0.94	>1.00 / >1.00	Avoids saturation
Lateral acceleration peak	28% lower	Moderate	Highest	48% lower vs API
Control energy	Lowest	Medium	Highest	Most efficient

The integrated comparison is listed in Table 4, which summarizes the performance measurement matrix across all evaluated criteria. The FPPC-API-NET demonstrates consistently superior results, achieving higher steering accuracy, stronger yaw stability, reduced sideslip, more balanced tire utilization, smoother lateral acceleration, and greater overall robustness. In contrast, the FTPPC-API delivers moderate performance with acceptable tracking and stability, whereas the API controller shows the weakest control quality, characterized by larger errors, slower convergence, and less effective dynamic regulation.

4. CONCLUSIONS

This study presents a proposed FPPC-API-NET for steering and yaw-motion regulation of RSV under varying inertial loads and aerodynamic disturbances. By integrating an FT-PPC framework with NET, the proposed controller ensures that tracking errors remain bounded within predefined decay envelopes, while the anti-windup compensation maintains actuator stability. Simulation results verify that FPPC-API-NET in RSV drive motion in the cornering path achieves the most accurate steering position tracking, reducing steady-state error by 68% compared to FTPPC-API and 95% relative to API, with faster convergence and minimal

overshoot. These improvements directly enhance yaw stability and path-following accuracy, yielding smaller lateral displacement errors, smoother yaw responses, and better overall dynamic coordination during cornering maneuvers.

The improved steering and yaw performance further enhance vehicle stability, as evidenced by reduced sideslip magnitude and rate, balanced tire friction utilization below saturation limits, and smoother lateral acceleration, with peaks up to 48% lower than the baseline. Robustness analysis confirms that FPPC-API-NET exhibits a 66.7% faster rise time, a 87.4% shorter transient duration, and a 70% faster settling time than FPPC-API, while maintaining tight prescribed performance bounds. These results establish FPPC-API-NET as a robust and efficient control scheme capable of sustaining high tracking precision and stability under varying inertia and disturbance conditions.

From an implementation perspective, the proposed FPPC-API-NET relies on algebraic nonlinear transformations and PI-based control structures, which are computationally lightweight and suitable for real-time embedded automotive controllers. Although the present study focuses on simulation-based validation, the control architecture is well-suited for practical deployment in steering systems with limited computational resources. Future work will focus on extending the controller to incorporate full vehicle dynamics, including roll motion and load transfer, followed by real-time experimental validation on an actual RSV platform with embedded hardware to assess performance under real-world uncertainties.

ACKNOWLEDGMENT

The authors would like to thank Universiti Malaysia Pahang Al-Sultan Abdullah (UMPSA) for providing financial support under the Postgraduate Research Grant No. PGRS200348 and for laboratory facilities.

REFERENCES

[1] El Hajjami, L., Mellouli, E. M., Žuraulis, V., & Berrada, M. (2023). A novel robust adaptive neuro-sliding mode steering controller for autonomous ground vehicles. Robotics and Autonomous Systems, 170, 104557, doi:10.1016/j.robot.2023.104557.

[2] Zhou, X., Wang, Z., Shen, H., & Wang, J. (2022). Robust Adaptive Path-Tracking Control of Autonomous Ground Vehicles With Considerations of Steering System Backlash. IEEE Transactions on Intelligent Vehicles, 7(2), 315-325, doi:10.1109/TIV.2022.3146085.

[3] Chen, G., Yao, J., Hu, H., Gao, Z., & Hua, M. (2024). Hierarchical Coupling Motion Control of Distributed Vehicle Considering Vehicle Posture. IEEE Transactions on Vehicular Technology, 73(8), 10899-10915, doi:10.1109/TVT.2024.3369923.

[4] Liang, J., Feng, J., Lu, Y., Yin, G., Zhuang, W., & Mao, X. (2024). A Direct Yaw Moment Control Framework Through Robust T-S Fuzzy Approach Considering Vehicle Stability Margin. IEEE/ASME Transactions on Mechatronics, 29(1), 166-178, doi:10.1109/TMECH.2023.3274689.

[5] Dong, E., Wang, F., Li, B., & Zhang, L. (2022) Vehicle lateral stability control based on sliding model in high-speed sharp turning condition. In 2022 International Seminar on Computer Science and Engineering Technology (SCSET), 8-9 Jan. 2022 2022 (pp. 183-186). doi:10.1109/SCSET55041.2022.00051.

[6] Yim, S. (2020). Comparison among Active Front, Front Independent, 4-Wheel and 4-Wheel Independent Steering Systems for Vehicle Stability Control. Electronics, 9(5), 798, doi:10.3390/electronics9050798.

[7] Rsetam, K., Khawwaf, J., Zheng, Y., Cao, Z., & Man, Z. (2024). Fast Finite-Time Composite Controller for Vehicle Steer-by-Wire Systems with Communication Delays. World Electric Vehicle Journal, 15(4). doi:10.3390/wevj15040132

[8] Zhou, S., Li, Y., & Tong, S. (2024). Prescribed performance adaptive fuzzy output feedback control for steer-by-wire vehicle system with intermittent actuator faults. Neural Comput. Appl., 36(26), 16057–16070, doi:10.1007/s00521-024-09797-6.

[9] Zhang, J., & Li, J. (2019). Integrated vehicle chassis control for active front steering and direct yaw moment control based on hierarchical structure. Transactions of the Institute of Measurement and Control, 41(9), 2428-2440, doi:10.1177/0142331218801131.

[10] Liang, J., Yin, G., & Li, G. (2018) Robust H∞ Output-feedback Vehicle Yaw Control Using an Active Front Wheel Steering. In 2018 37th Chinese Control Conference (CCC), 25-27 July 2018 (pp. 7760-7764). doi:10.23919/ChiCC.2018.8483289.

[11] Alturky, L., & Khawwaf, J. (2025) Precision Tracking for Steer-by-Wire Systems Based on Fast Integral Terminal Sliding Mode Control. In 2025 5th International Conference on Emerging Smart Technologies and Applications (eSmarTA), 5-6 Aug. 2025 2025 (pp. 1-8). doi:10.1109/eSmarTA66764.2025.11132223.

[12] Yang, R., & Liao, D. (2025). Fault-Tolerant Control of Steer-by-Wire System Based on Sliding Mode Observer With Neural Network. IEEE Access, 13, 134831-134845, doi:10.1109/ACCESS.2025.3593492.

[13] Gao, Z., Liu, W., Wei, Z., & Guo, G. (2025). Adaptive Finite-Time Prescribed Performance Control of Vehicular Platoons With Multilevel Threshold and Asymptotic Convergence. IEEE Transactions on Intelligent Transportation Systems, 26(5), 6503-6513, doi:10.1109/TITS.2025.3536002.

[14] Nguyen, N. T., Le, D. T., Dang, V. T., Pham, V. H., Nguyen, D. H., Hoang, D. C., et al. (2022) Prescribed Tracking Performace for Lateral Control of an Autonomous Vehicle with High-Gain Observer. In 2022 11th International Conference on Control, Automation and Information Sciences (ICCAIS), 21-24 Nov. 2022 2022 (pp. 158-163). doi:10.1109/ICCAIS56082.2022.9990307.

[15] Wang, P., Feng, T., Song, C., Li, J., & Yang, S. X. (2025). A Study of the Stability of an Industrial Robot Servo System: PID Control Based on a Hybrid Sparrow Optimization Algorithm. Actuators, 14(2), 49, doi:10.3390/act14020049.

[16] Afrianto, A., Heryadi, B., Dewi, D. K., Wiranata, T., Rahman, H. A., Nurprasetio, I. P., et al. (2025). Experimental Investigation of PID Control Strategy for Three-Phase Induction Motor Speed Control System Implemented on a Scaled Railway Vehicle Roller Test Rig Driver. International Journal of Sustainable Transportation Technology, doi:10.31427/IJSTT.2025.7.1.1.

[17] Azahar, M. I. P., Irawan, A., & Ramli, M. S. (2020) Finite-Time Prescribed Performance Control for Dynamic Positioning of Pneumatic Servo System. In 2020 IEEE 8th Conference on Systems, Process and Control (ICSPC), 11-12 Dec. 2020 2020 (pp. 1-6). doi:10.1109/ICSPC50992.2020.9305755.

[18] Bian, M., Chen, L., Luo, Y., & Li, K. (2014). A Dynamic Model for Tire/Road Friction Estimation under Combined Longitudinal/Lateral Slip Situation (Vol. 1, SAE Technical Papers).

[19] Bhoraskar, A., & Sakthivel, P. (2017) A review and a comparison of Dugoff and modified Dugoff formula with Magic formula. In 2017 International Conference on Nascent Technologies in Engineering (ICNTE), 27-28 Jan. 2017 2017 (pp. 1-4). doi:10.1109/ICNTE.2017.7947898.

[20] Fawzan Khaizuran, F., & Irawan, A. (2020). Steering Angle Control of Rack Steering Vehicle using Antiwindup-PI-Control. International Journal of Electrical Engineering and Applied Sciences (IJEEAS), 3(1).